Journal of Energy Storage 78 (2024) 110049

Contents lists available at ScienceDirect

Journal of Energy Storage

journal homepage: www.elsevier.com/locate/est

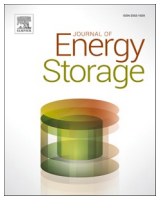

Research Papers

The effect of lithium battery overpotential on sulfurized-polyacrylonitrile (SPAN): A theoretical approach

Samuel Bertolini [a,b,*], Pedro Venezuela [a], Arnaud Delcorte [b]

[a] Institute of Physics, Universidade Federal Fluminese (UFF), Av. Gal. Milton Tavares de Souza, s/n° - Campus da Praia Vermelha, 24210-346 Niteroi, Rio de Janeiro, Brazil

[b] Universite Catholique de Louvain, 1 Croix du Sud, B1348 Louvain-la-Neuve, Belgium

ARTICLE INFO

Keywords:
Density functional theory
Sulfurized-polyacrylonitrile
Overpotential reaction
Lithium-sulfur batteries

ABSTRACT

The use of SPAN as a positive electrode for lithium-sulfur batteries (LiSB) has demonstrated that, the material preserves a high specific capacity for several cycles. Through the recharging cycle, e.g. in Li-ion batteries, overpotential reactions can occur and promote degradation of the electrode material. In this work, we investigate the overpotential reactions that may occur in the presence of SPAN and cyclized-polyacrylonitre (cPAN). To approach this, ab initio molecular dynamics (AIMD) was used, and depletion of electrons was created in the system, thus inducing overpotential reactions in SPAN and cPAN. The simulations indicate that overpotential reactions tend to degrade the system, enabling reactions between the polymer and the solvent, as well as generating new branches in the polymer due to interactions with solvent radicals. The presence of different salts can also impact the overpotential reactions either by reacting with the solvent or by necessitating higher overpotential values.

1. Introduction

In contemporary society, electronic storage devices are become predominant and serve a wide range of purposes, including laptops, electric vehicles, toys, and renewable energy systems [1]. Among these devices, lithium-ion batteries have emerged as the dominant commercial solution for energy storage, which has led to numerous research efforts and advancements in this field [2]. However, lithium-ion batteries are approaching their theoretical capacity limit, prompting the exploration of alternatives to enhance the specific capacity of batteries. This involves considering the replacement of either the negative electrode (e.g., lithium metal) or the positive electrode (e.g., conversion electrodes) [3–7]. In the case of lithium batteries, sulfur cathodes have emerged as a promising candidate for replacing lithium-ion batteries due to their high specific capacity. Nevertheless, despite the higher specific capacity offered by lithium-sulfur batteries, there are still certain challenges that hinder their widespread commercial application. The primary obstacles include self-discharge and degradation of the anode, caused by the migration of polysulfides (PSs) within the battery system [8–10].

The PSs are formed during the lithiation of the sulfur until the precipitation of insoluble salts on the positive electrode (sulfur cathode), which is Li_2S_2 and Li_2S. Until the sulfur chains are not completely lithiated, the PSs can be soluble in the electrolyte. Thus, the shuttle of the PSs are promoted by their solubility on the electrolyte and migration to the negative electrode (lithium anode) [11,12]. Consequently, the main strategies to reduce or eliminate the shuttle of PSs are: to confine, hold or catalyze the PSs until it converts into Li_2S inside the cathode. Therefore, the common tactics are modifying the host material (graphite): modifying the architecture of the graphite as a host material [13–17], use of adatom on the graphite [18,19], adding additives on the graphite [20–23], and using membranes to stop polysulfide migration [24–27]. Graphite is used as host material because lithium sulfides do not conduct electricity, however, the interactions between the graphite and sulfur are through van der Waals interactions, therefore, weaker than chemical interactions. A most sophisticated strategy is to replace the use of graphite with sulfurized polyacrylonitrile (SPAN), in such a way sulfur is chemically adsorbed and can conduct electricity [28–33].

The SPAN is produced from the synthesis of polyacrylonitrile with α-sulfur at temperatures around 500 °C, where sulfur chemically bonds to the polymer [34,35]. The synthesis is similar to the production of carbon fibers from polyacrylonitrile, where a cyclized polyacrylonitrile

* Corresponding author at: Institute of Physics, Universidade Federal Fluminese (UFF), Av. Gal. Milton Tavares de Souza, s/n° - Campus da Praia Vermelha, 24210-346 Niteroi, Rio de Janeiro, Brazil.

E-mail addresses: samuel.bertolini@uclouvain.be (S. Bertolini), pedrovenezuela@id.uff.br (P. Venezuela), arnaud.delcorte@uclouvain.be (A. Delcorte).

https://doi.org/10.1016/j.est.2023.110049
Received 1 September 2023; Received in revised form 10 November 2023; Accepted 6 December 2023

(cPAN) is formed as an intermediary, and H_2 is eliminated from the process [36–39]. In presence of sulfur, SPAN is formed and HS_2 is eliminated from the process. The structure of the SPAN backbone is proposed as π-conjugated, in a preferential stair-like backbone, with sulfur chains attached to the polymer, in a such configuration that the π-conjugated system allows the polymer to conduct electricity [40–43].

Within lithium-sulfur batteries (LiSB), the incorporation of SPAN as a host material has shown to extend battery lifespan in comparison to graphite hosts, as well as preventing the detection of polysulfides in certain solvents [44–48]. Furthermore, various approaches have been explored to enhance battery performance, particularly conductivity, through the utilization of additives [49–52]. The synthesis process can result in incomplete reactions between sulfur and the polymer, leading to the formation of undercoordinated carbon (Cuc) [53]. Additionally, the cleavage of C—S bonds during battery cycles can give rise to the presence of Cuc within the polymer structure [54]. Due to its pseudo-capacitance and semi-conductance [55], SPAN exhibits a greater specific capacity in comparison to traditional carbon/sulfur electrodes. This increase in capacity is primarily attributed to the reduction of graphite as a host material. Moreover, SPAN demonstrates a higher capacity than the theoretically expected 1675 mAh g^{-1}. The potential sources of this specific capacity enhancement include increased lithiation through Li ion intercalation [31,56], the adsorption of Li ions by the N atoms [57,58], or the cleavage of C—S bonds. Notably, the initial capacity of SPAN can achieve 1843 mAh g^{-1} and retains over 1000 mAh g^{-1} even after 1000 cycles [54,59].

Based on our previous studies, we have observed that Cuc or a single sulfur atom attached to Cuc can capture soluble polysulfides, and the presence of Cuc tends to diminish during initial battery cycles as it reacts with the solvent. This behavior is influenced by the structure of the SPAN backbone [60,61]. Moreover, our simulations indicate a direct correlation between the structure of SPAN and the battery's performance [57,62]. In this research, our focus is to examine the impact of overpotential on Lithium-Sulfur batteries (LiSB) when SPAN is employed as the positive electrode during the battery's recharging process. The overpotential has the capacity to induce reactions on the host material, potentially leading to the formation of a cathode electrolyte interphase (CEI). To shed light on the overpotential reactions, we have utilized different salts within the same solvent, as well as different configurations of SPAN.

During the battery charging process, two distinct half-reactions occur at the positive and negative electrodes. In the negative electrode, an electric field is applied to the system, compelling lithium ions to deposit within the solid-electrolyte interphase (SEI), subsequently migrate from the SEI to reach the metal/SEI interface, where they gain electrons, resulting in the reduction of lithium ions to form lithium metal. In the positive electrode, various competing phenomena take place. These include the removal of lithium ions from the electrode, the dissolution of lithium ions from sulfur into the electrolyte, and the extraction of electrons from the system. In this context, the electric field facilitates the extraction of both electrons and lithium ions from the positive electrode. Therefore, our investigation focuses on the overpotential reactions that arise due to a localized depletion of electrons in the positive electrode, leading to the transfer of electrons from the positive electrode to the negative electrode, based on the half-reaction $Li^+ + e^- = Li$.

2. Computational methods

The simulations used density functional theory (DFT) performed by Vienna Ab initio Simulation Package (VASP), employing plane waves basis set described by projector-augmented-wave pseudopotentials, treated by the generalized gradient approximation functional proposed by Perdew, Burke, and Ernzerhof (PBE), and energy cutoff of 400 eV. The Brillouin zone was sampled with a Monkhorst–Pack mesh of 1 × 1 × 1 k-points, and van der Waals dispersion corrections were added using DFT-D3 approximation in the Becke–Johnson formulation. Ab-Initio molecular dynamics (AIMD) are carried out in the canonical ensemble (NVT) at 330 K using a time step of 1 fs, and all charge analyses were calculated on the basis of Bader charges. All further parameters were set by the default value [63–73].

To represent a continuous SPAN backbone immersed in the electrolyte, we used the periodic boundary conditions to connect the bottom and top parts of the polymer backbone. Two different polymer structures, one representing cPAN, and another SPAN with two PSs (Li_2S_3) attached to SPAN in their relaxed configuration. Then the electrolytes were filled into the cell, maintaining the same density of the electrolyte which is 1.06 g/cm^3. The electrolyte is composed of 1,3-dioxolane (DOL) and the salt. Dissolved in the electrolyte 1 mol of lithium bis(trifluoromethane sulfonyl)imide (LiTFSI) or 2 mol of lithium bromide (LiBr) were used as salt, due to the LiBr ability to produce a CEI [74]. The simulations cell has a constant volume of 15.0 × 18.0 × 18.5 Å, and consequently, 4 different systems were built (Fig. 1): SPAN with LiBr, SPAN with LiTFSI, cPAN with LiBr, and cPAN with LiTFSI, as indicated on Table 1. The cPAN can be the symbol part of the polymer that has not been reacted with sulfur. While the sulfur content within SPAN does indeed influence battery performance [74], the arrangement of cPAN and SPAN signifies not a precise sulfur content in the electrode, but rather a representation of the localized polymer structures found in an actual SPAN cathode. This representation accounts for regions with sulfur and those devoid of sulfur.

The overpotential was simulated by removing one electron from the system every 2.5 ps in a total of 10 electrons, and then one electron was added to the system every 2.5 ps until neutralization of the system, to posterior relaxation of the system for more 2.5 ps. The charge of the system over time is shown in Fig. S1. Additionally, all-electrons DFT calculations using def2-TZVP basis set and M062X method were performed by Orca Software 5.1 [75,76].

3. Results

When an electron is extracted from the system to represent an overpotential, the system's energy increases. This increase in energy indicates an unfavorable thermodynamic behavior, and therefore the removal of electrons depends on the anode half-reactions. In the case of a lithium battery, it takes approximately 1.4 eV of energy to reduce one electron in the lithium metal anode, as half-reaction of $Li^+ + e^- = Li$ [77]. If the energy required to remove an electron from the system exceeds 1.4 eV, it enters an overpotential regime. As shown in Fig. 2A, a simulation time of 2.5 ps is insufficient to fully relax the system's energy, causing the system's energy to scale faster. In a realistic overpotential scenario, the system also tends to continually move out of equilibrium, but our simulations may exhibit artifacts such as accelerated kinetic reactions due to an excessive charge on the system. Furthermore, in DFT simulations, the removal or addition of electrons tends to be distributed throughout the entire solvent rather than restricted to a single molecule. Therefore, the system requires more time or a higher charge to decompose, as observed in the lithium-metal anode [78]. Nonetheless, it is possible to observe differences in the energy required to release an electron to the counter electrode between cPAN and SPAN (Fig. 2B).

In the presence of cPAN, it is necessary approximately 0.6 eV of overpotential to remove one electron from the system, while it is possible to remove electrons from SPAN system below the overpotential limit. As mentioned in preview studies, the polysulfide transfers charge to the polymer backbone [60,61], therefore the negative charge of the polymer backbone could facilitate the removal of electrons from the system. In the case of SPAN, the energy to remove one electron increases proportionally to the number of electrons removed, and the energy to remove electrons are below the overpotential reference (Li anode) up to a total of 4 electrons removed from the system. The reference of 1.4 eV is the half charge reaction to reduce Li ion, here used as counter-electrode. This can be associated with the amount of Li atoms that were absorbed

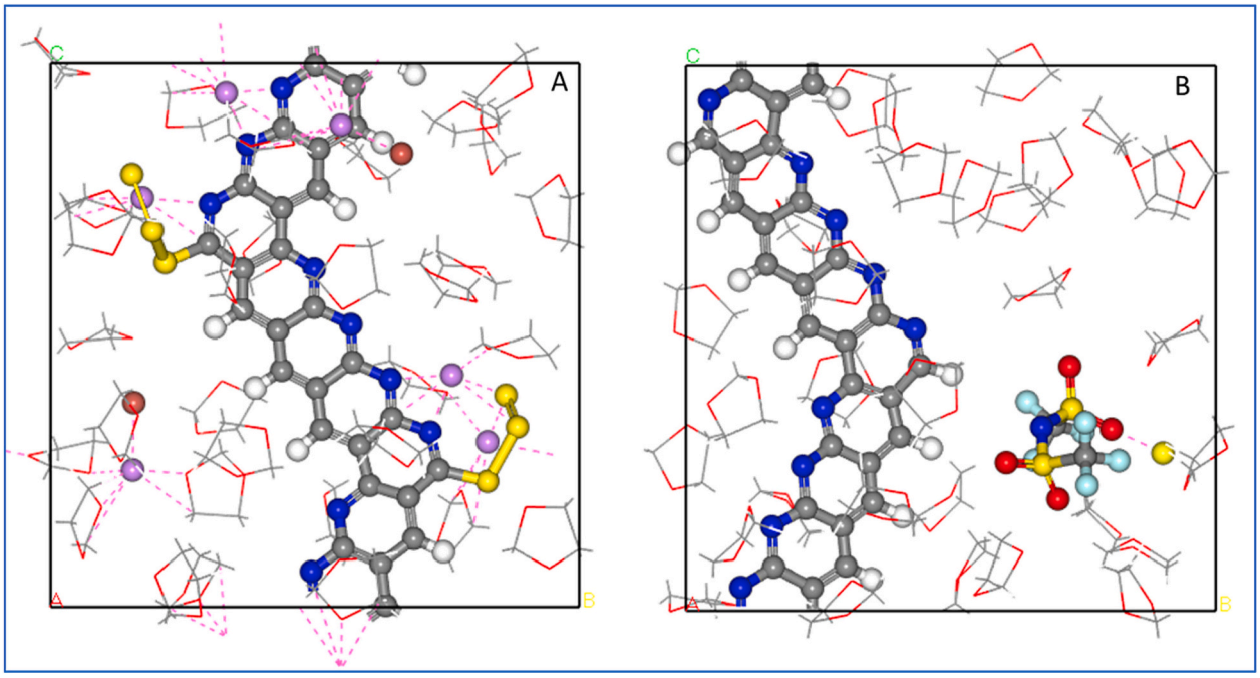

Fig. 1. System's representation, containing one type of salt (LiBr or LiTFSI) and the polymer backbone. A) SPAN is the polymer and B) cPAN is the polymer.

Table 1
Composition of each system simulated.

#	DOL	SPAN	PAN	LiTFSI	LiBr
System 1	32	1	0	1	0
System 2	32	1	0	0	2
System 3	32	0	1	1	0
System 4	32	0	1	0	2

during the PS capturing process (4 Li atoms), representing a single dissolution of the Li-ions. However, even after 4 electrons were removed from the SPAN systems, the overpotential tends to be smaller than in the presence of cPAN (Fig. 2B).

The salt also appears to produce an effect on the overpotential of the system during the removal of electrons. Comparing LiBr and LiTFSI, the system's energy tends to increase faster in the presence of LiTFSI than in the presence of LiBr, although they have similar overpotential values (~0.6 eV). Another difference is during the reneutralization period (adding electrons) in the presence of SPAN, where the energy profile change between the presence of LiBr and LiTFSI (Fig. 2A). This can be observed after 30 ps of simulation (when 3 electrons are replaced in the system containing SPAN), and in the presence of LiBr the energy of the system increases, while in the presence of LiTFSI decreases until it becomes relatively constant. Because the energy of the system tends to increase when electrons are reintroduced into the system, this indicates that the system prefers to maintain positive charges. As indicated in Fig. 2A, after ~32 ps for the electrolytes containing LiBr, and after 38 ps for the electrolytes with LiTFSI, the total energy increases when electrons are added to the cells during neutralization of the system. Due to the reactions that take place during overpotential, the system tends to favor the retention of positive charges during neutralization. The products resulting from overpotential reactions will carry a charge, thereby compelling the cathode to maintain a positive charge. As a result, it is anticipated that the voltage of the battery will be influenced following overpotential reactions.

The reactions observed in the system containing SPAN and LiBr are summarized in Fig. 3, and the charge distribution is in Table 2. At 15.2 ps of simulation, DOL will release one H atom to react with the edge of the sulfur chain, forming a 2-hydro-1,3-dioxolane (HDOL) and hydro-sulfurized-polyacrylonitrile (HSPAN) at 15.4 ps of simulation, as described by the schematic Reaction 1. At 20.2 ps in a system charged 8.0 |e|, DOL reacts with Br to obtain HBr and HDOL as products (20.4 ps), as proposed by Reaction 2. Similar to Reaction 1, at 20.8 ps in a system charged 8.0 |e|, a DOL supplies one H atom to the second sulfur chain, forming dihydro-sulfurized-polyacrylonitrile (H2SPAN, see Fig. 3), as proposed by the Reaction 3. During the regime that electrons were reintroduced into the system, between 39.4 and 39.5 ps (system charge of 3|e|), HDOL bonds to the polymer backbone, forming a new ramification named DH2SPAN (see Fig. 3), as proposed by Reaction 4. When a new electron is added to the system (time and charge of 40.5 ps and 2|e| respectively), one sulfur chain is completely removed from the system as suggested on Reaction 5, forming a solvated HS_3 and one a polymer backbone with 1 sulfur chain attached and 1 HDOL also attached, therefore named DHSPAN (see Fig. 3). Also, at 41.5 ps in a system charge of 2 |e|, the other sulfur chain is partially detached, creating a solvated HS_2, and maintaining the polymer backbone with one sulfur atom, here named DSPAN (see Fig. 3) as proposed by Reaction 6. Finally, at 41.8 ps (system charge of 2 |e|), another HDOL bonds to the sulfur in the polymer backbone, henceforth named D2SPAN (see Fig. 3), as suggested by Reaction 7. No further reactions were observed during the simulation, even when electrons were added until the system became neutral.

Reaction 1) $DOL + SPAN^{+} = HDOL^{+} + HSPAN$
Reaction 2) $DOL + Br^{-} = HDOL^{+} + HBr$
Reaction 3) $DOL + HSPAN = HDOL^{+} + H2SPAN$
Reaction 4) $HDOL^{+} + H2SPAN^{3-} = DH2SPAN^{2-}$
Reaction 5) $DH2SPAN^{3-} + e^{-} = HS_3^{-} + DHSPAN^{3-}$
Reaction 6) $DHSPAN^{3-} = HS_2^{-} + DSPAN^{2-}$
Reaction 7) $DSPAN^{2-} + HDOL^{+} + e^{-} = D2SPAN^{-2}$
Reaction 8) $SPAN = SPAN\_NS^{+} + e^{-}$

The Bader charge of Li and Br as ions can oscillate but tend to be constant over time, where each Li ion tends to have a charge of 0.87 |e| and each Br ion of −0.75 |e|. The removal of electrons is distributed between the solvent and the polymer backbone. It could be expected

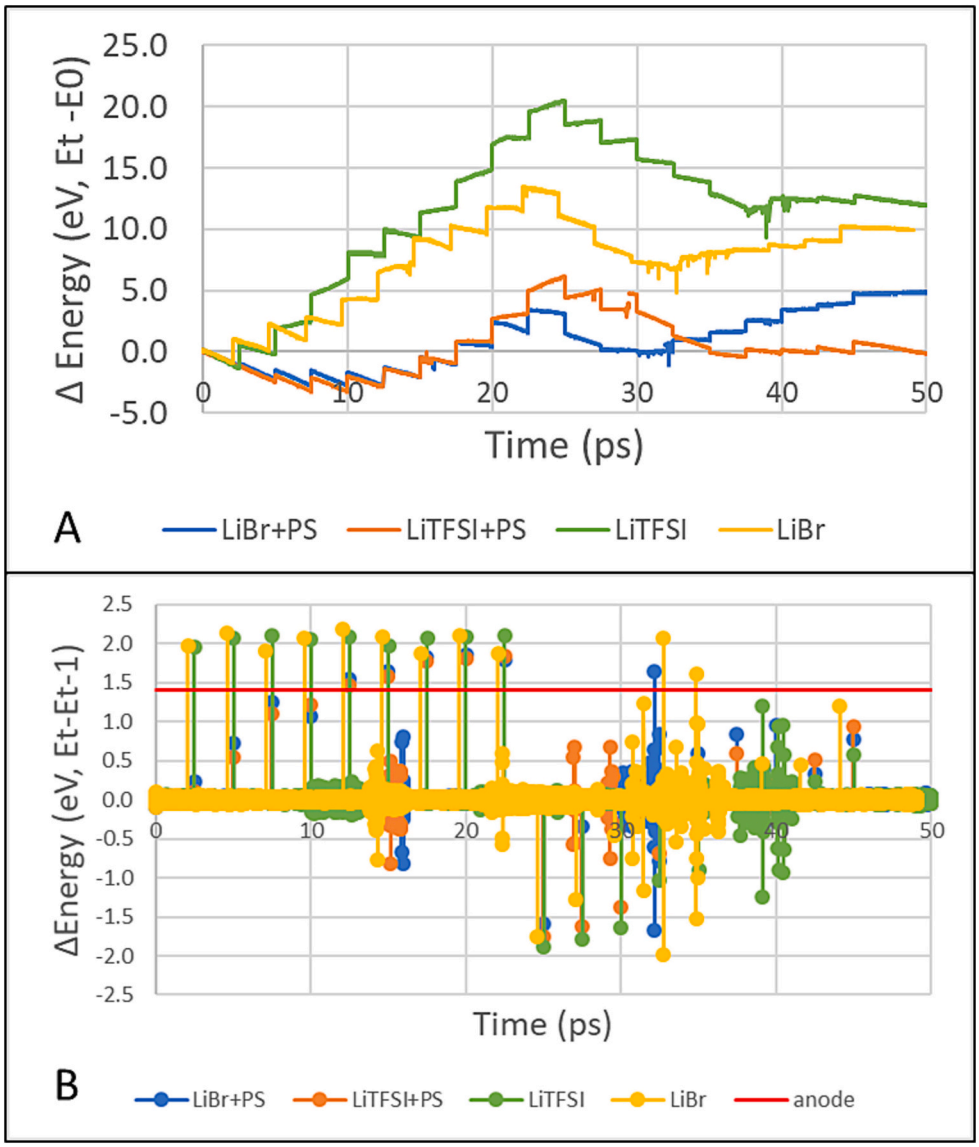

Fig. 2. Overpotential energy profile over time. A) Initial state as energy reference (E[i] − E[o]); and B) last state energy frame as reference (E[i] − E[i − 1]).

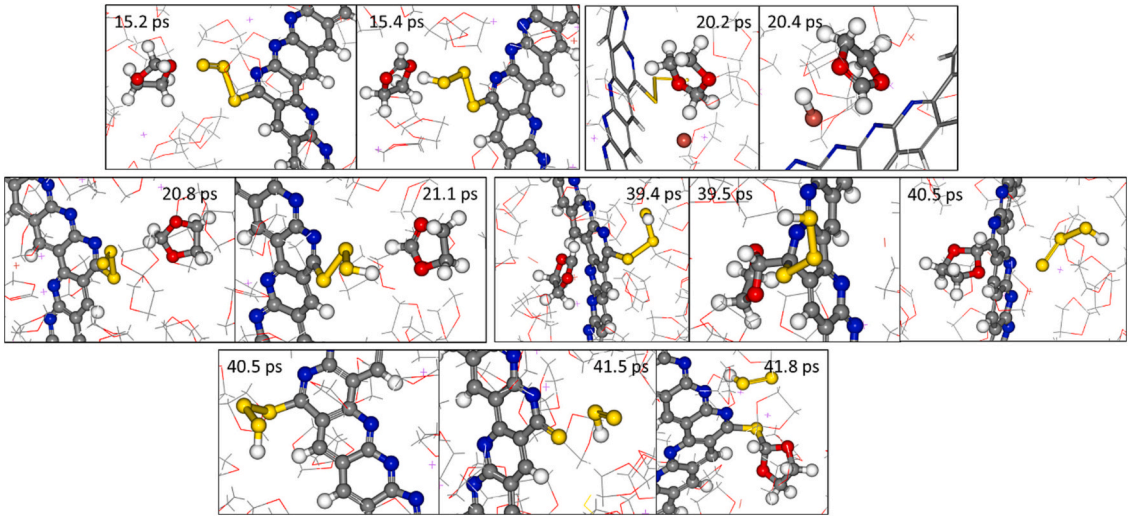

Fig. 3. Reactions frames over time, in the system containing SPAN and LiBr. Color code: H is white, C is gray, N is blue, O is red, S is yellow, and Br is brown. (For interpretation of the references to color in this figure legend, the reader is referred to the web version of this article.)

Table 2
Charge evolution of the molecules over time in a system containing SPAN and LiBr.

15.2 ps		15.4 ps		20.2 ps		20.4 ps		20.8 ps		21.1 ps		39.4 ps		39.5 ps		40.5 ps		41.5 ps		41.8 ps	
DOL	0.18	HDOL	0.86	DOL	0.40	HDOL	0.90	DOL	0.13	HDOL	0.87	HDOL	0.51	DH2SPAN	−2.49	DHSPAN	−2.77	DSPAN	−2.39	D2SPAN	−1.99
SPAN	1.05	HSPAN	0.63	Br*	−0.45	HBr	0.04	HSPAN	0.41	H2SPAN	0.24	H2SPAN	−2.92	–	–	HS3	−0.52	HS2	−0.49	HS2	−0.57
Li	5.26	Li	5.22	Li	5.26	Li	5.29	Li	5.28	Li	5.23	Li	5.25	Li	5.21	Li	5.19	Li	5.24	Li	5.22
Br	−1.46	Br	−1.42	Br	−0.71	Br	−0.78	Br	−0.80	Br	−0.82	Br	−0.67	Br	−0.72	Br	−0.70	Br	−0.72	Br	−0.63
Solv.	0.97	Solv.	0.70	Solv.*	2.89	Solv.*	2.05	Solv.**	2.96	Solv.**	2.45	Solv.**	1.00	Solv.**	1.10	Solv.**	0.93	Solv.**	1.09	solvents*	0.69
–	–	–	–	HSPAN	0.60	HSPAN	0.50	HBr	0.03	HBr	0.03	HBr	−0.17	HBr	−0.09	HBr	−0.14	HBr	−0.11	HBr	−0.20
–	–	–	–	–	–	–	–	–	–	–	–	–	–	–	–	–	–	HS3	−0.63	HS3	−0.53
System 6.00		System 6.00		System 8.00		System 8.00		System 8.00		System 8.00		System 3.00		System 3.00		System 2.00		System 2.00		System 2.00	

that removing one electron without inducing a reaction is an artifact of the method used because the electron is not confined in the orbital of the same molecule. The charge of the solvent (Solv., Table 2) also contains ions (e.g. Solv.** contains two $HDOL^{+}$), thus one DOL molecule tends to decompose when the change of the solvent tends to 1.0 |e|. Comparing the charge of the solvent and the DOL molecule that decomposes at 15.2 ps, the solvent is charged, but DOL tends to be neutral. When the first reaction occurs with SPAN at 15.2, the polymer has a positive charge of 1.05 |e|, but after this, the charge of the polymer continuously decays, becoming negative, which indicates that the polymer is a reservoir of electrons. The Li ions absorbed in the SPAN also contribute to the amount of electrons inside of the polymer backbone. In this case, the increase of energy below the overpotential values indicates to be due to Li-ions solvation. Considering the SPAN as a reservoir of electrons, a higher charge cathode tends to be less reactive against the overpotential effect than a more discharged cathode.

When the system contains LiTFSI and SPAN, overpotential reactions between DOL and SPAN can occur, but the LiTFSI does not participate in the reactions, as summarized in Fig. 4. Additionally, the system starts to react after a longer time of simulation when compared with LiBr and SPAN systems (23.3 vs 15.2 ps). The first observed reaction that happens is the enclosure of the sulfur ring to the polymer backbone and forming a NS bond (Reaction 8), during this time, the system has 9 electrons removed. After the first electron is removed from the whole solvent, the DOL supplies one H to the SPAN, creating an HS bond, similar to Reaction 1. At 37.5 ps of simulation in a charging system of 4 |e|, the enclosed sulfur chain breaks by cleavage in the SS bond. When the system has a charge of 1 |e|, at 42.4 ps, the H is transferred on the SPAN backbone, from S to N, breaking a HS bond to create a HN bond. Finally, when the system is neutral, at 46.9 ps of simulation, HDOL gets attached to the SPAN in a reaction similar to Reaction 4. In the system that contains SPAN and LiBr, tree HDOL were formed during simulation, while in the system that contains SPAN and LiTFSI, only one HDOL appears; additionally, no PS was removed from the polymer structure.

The charge variations of different structures of the system that contain SPAN and LiTFSI are shown in Table 3. When the reaction is a modification in the structure of the polymer, there is no change in charge from the reactant (SPAN) to the product (SPAN!). The salt (TFSI) and Li ions had constant charges during the whole simulation, where the TFSI has a charge of −0.93 |e|. Independent of the salt used in the simulations, the electrons extracted from the system will be removed from the polymer and the solvent. In other hand when the salt is LiBr, in the presence of LiTFSI, the solvent can accumulate positive charge up to 4 |e| without decompose. Since LiTFSI does not participate in the reactions or transfer charge, the reactivity could be correlated with the solvation structure. Similarly in the presence of LiBr, in the presence of LiTFSI, the electrons were removed from the SPAN, and later the polymer gained electrons while the system went back to neutrality.

When sulfur is not present in the structure of the backbone, the solvent will react with the polymer backbone (Figs. S2–S3), supplying H atoms to form HN bonds on the cPAN and HDOL dissolved in the electrolyte. Because S is not present in the system, N atoms in the polymer will react with the H atoms from the solvent or with the solvent missing one H atom. In the presence of LiBr, the salt will also react with the solvent to form HBr, while LiTFSI does not react. Also, in the presence of HDOL after the charge is equilibrated, the molecule tends to attach to the polymer backbone, forming a new ramification on the polymer. This ramification can occur on the N or C of the cPAN backbone. Additionally, similar to in SPAN, reactions tend to occur in a short simulation time in the presence of LiBr compared to the time in the presence of LiTFSI (4.8 vs 10.0 ps). Reactions also tend to be faster in the presence of cPAN than in SPAN, which can be associated with the different amounts of Li ions present in the simulation. The polymer tends to behave as a reservoir of electrons and the presence of Li increases the amount of electrons in the polymer. Thus, the simulations suggest that overpotential tends to reduce reactions in more lithiated stages of the

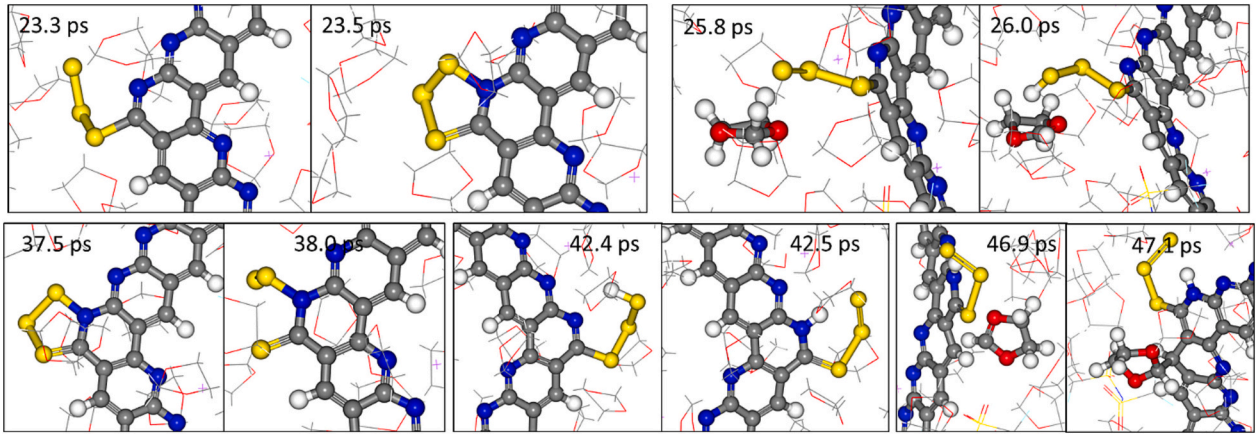

Fig. 4. Reactions frames over time, in the system containing SPAN and LiTFSI. Color code: H is white, C is gray, N is blue, O is red, S is yellow, and Br is brown. (For interpretation of the references to color in this figure legend, the reader is referred to the web version of this article.)

discharge process. Moreover, once one electron is removed from the DOL, the reaction to supply H atom to the Br is thermodynamically more favorable than the supply of H atoms to the polymer (−81.7 vs −62.6 kcal/mol).

4. Discussion

The overpotential in batteries can lead to the decomposition of the electrolyte and irreversible phase transformation and failure of the cathode. Some salts such as LiBr under the conditions of overpotential can react with the solvent, promoting the formation of a cathode electrolyte interphase (CEI) [79,80]. In our simulations, the salt will also have relevance in the overpotential reactions with the solvent, e.g. LiBr removes H atoms from the DOL, while LiTFSI does not react with the solvent or the polymer backbone. Experimental analyses should be investigated to better understand the behavior of LiBr in SPAN. Nevertheless, in the presence of LiTFSI, overpotential reactions also occur, and the solvent supplies H atoms to the polymer backbone. In preview studies, we observed that removal of H from the solvent happens preferentially in specific sites of the solvent structure, and also deprotonation is more favorable in solvents than in the SPAN [57]. This work is in agreement with preview studies, here the DOL is only deprotonated in the same H location, therefore forming HDOL, while the polymer (cPAN and SPAN) receives hydrogen from the solvent. Additionally, overpotential reactions can be reduced by replacing the solvent, and using solvents that are more resistant to deproteination. Overpotential is a mechanism of solvent decomposition and cathode degradation, produced by oxidative reactions in different solvents that can induce hydrogen transference [81–83].

In our preview simulations, we observed that N in cPAN adsorbs Li atoms from the polysulfide [60–62]. Because of the overpotential, DOL supplies H to the polymer, forming N—H bonds, this result suggests that overpotential tends to irreversibly degrade the positive electrode and also reduce the specific capacity of the battery. The sites available to lithiation tend to permanently disappear when an overpotential reaction occurs, forming N—H bonds. In this perspective, salts such as LiBr may protect or reduce SPAN during an overpotential, where Br protonates instead of the polymer. While LiTFSI indicates to reduce the probability of the solvent react due to changes in the solvation structure. Furthermore, when the system is again neutralized and the overpotential is reduced, HDOL can react with the polymer, creating new ramifications on the polymer structure. This ramification on SPAN may act as a site for absorbing Li-ions, a site for capturing PSs, and also is a way to confine dissolved PSs inside the cathode, however this should be further verified. The presence of HDOL and it reactions with SPAN are indications that a CEI should be formed in the presence of overpotential. Nevertheless, the formation of C—S between the reaction of HDOL and SPAN is an indication that part of the sulfur can be permanently lost in the formation of new ramifications on the SPAN backbone. The formation of radicals contain S and H is an indications that overpotential reactions could possible deliver the formation of H_2S, which is a toxic gas that could be released if the battery is damaged.

The formation of N—S bonds was detected in SPAN after synthesis and by DFT calculations [56,84,85]. Here we observe the formation of N—S bonds due to the presence of overpotential. Although the overpotential, that creates N—S, should also affect the voltage of the battery. When the overpotential occurs, during charge and discharge, the reactions may be reversible, where the formation of Li_2S or N—S bonds can reversible be formed [85].

In presence of the sulfur chains attached to the polymer, therefore comparing SPAN and cPAN, the edge of the PSs will be a preferential site to chemisorb H eliminated from DOL during the overpotential reactions; while in cPAN, the N will be the preferential site. The overpotential will also facilitate the formation of PSs dissolved in the electrolyte because, after the chemisorption of H, the sulfur chain is removed from the polymer chain. Nevertheless, as observed in previous works, the dissolved PSs can be captured by the SPAN backbone [60–62]. Consequentially, during an overpotential reaction, the formation of a PS can be used as a sacrifice against the irreversible degradation of the polymer backbone.

The nature of the solvent would probably affect the overpotential reactions. First, because of different solubility of the PSs in different solvents, e.g. in carbonate solvents PS formation was not detected during cycles of SPAN. Second, because of the capacity of the solvent to supply hydrogen to SPAN in the presence of an overpotential.

5. Conclusion

During the recharge process, when electrons are extracted from SPAN and cPAN due to overpotential voltage, the system can undergo overpotential reactions. These reactions occur when the change in energy surpasses the overpotential threshold and involve interactions between the solvent and salt, or the solvent and polymer. As electrons are depleted, the solvent provides hydrogen (H) atoms to the polymer or salt (LiBr). These H atoms then react with the sulfur chain in the polymer or the nitrogen (N) atoms in the polymer backbone. These reactions reduce the available sites for lithiation, remove sulfur from the polymer, and degrade the polymer. The decomposed species of the solvent (HDOL) have a tendency to react with the polymer backbone, leading to the formation of new ramifications during system neutralization. In general, overpotential reactions in SPAN and cPAN are expected to negatively impact the battery's cyclability. However, the formation of new

Table 3
Charge evolution of the molecules over time in a system containing SPAN and LiTFSI.

23.3 ps		23.5 ps		25.8 ps		26.0 ps		37.5 ps		38.0 ps		42.4 ps		42.5 ps		46.9 ps		47.1 ps	
SPAN(SS)	1.46	SPAN(SNS)	1.74	SPAN	1.46	HSPAN	1.32	SPAN(SNS)	−0.66	SPAN(NS)	−1.58	HSPAN(HS)	−2.24	HSPAN(HN)	−2.34	HSPAN	−3.54	DHSPAN	−3.31
Solv.	4.04	Solv.	3.75	DOL	0.41	HDOL	0.80	Solv.*	1.22	Solv.*	1.19	Solv.*	0.80	Solv.*	0.93	HDOL	0.27	Solv.	−0.09
TFSI	−0.90	TFSI	−0.91	TFSI	−0.91	TFSI	−0.90	TFSI	−0.93	TFSI	−0.95	TFSI	−0.95	TFSI	−0.95	TFSI	−0.95	TFSI	−0.96
Li	4.41	Li	4.42	Li	4.42	Li	4.42	Li	4.36	Li	4.35	Li	4.38	Li	4.36	Li	4.35	Li	4.35
				Solv.	2.62	Solv.	2.36									Solv.	−0.13		
System 9.00		System 9.00		System 8.00		System 8.00		System 4.00		System 3.00		System 2.00		System 2.00		System 0.00		System 0.00	

ramifications in the polymer could have a positive effect.

LiBr acts as a sacrificial salt against polymer decomposition by reacting with the solvent to produce HBr, which in turn leads to the creation of HDOL and the formation of new ramifications on the polymer. This process helps in the formation of a CEI. Additionally, LiTFSI, another salt, appears to reduce the likelihood of overpotential reactions occurring.

CRediT authorship contribution statement

Samuel Bertolini: Conceptualization, Methodology, Modeling.
Pedro Venezuela: Conceptualization.
Arnaud Delcorte: Supervisor.

Declaration of competing interest

The authors declare the following financial interests/personal relationships which may be considered as potential competing interests: Samuel Bertolini reports financial support was provided by Carlos Chagas Filho Foundation for Research Support of Rio de Janeiro State.

Data availability

Data will be made available on request.

Acknowledgments

The support from Fundação Carlos Chagas Filho de Amparo à Pesquisa do Estado do Rio de Janeiro (FAPERJ) through Project ID E-26/200.602 and 210.366/2022 is gratefully acknowledged. The authors also acknowledge the computer time supported by the Institut de Calcul Intensif et de Stockage de Masse (CISM) at Université Catholique de Louvain.

Appendix A. Supplementary data

Supplementary data to this article can be found online at https://doi.org/10.1016/j.est.2023.110049.

References

[1] G. Pistoia, Lithium-ion Batteries: Advances and Applications, 2013.
[2] M. Rouholamini, C. Wang, H. Nehrir, X. Hu, Z. Hu, H. Aki, B. Zhao, Z. Miao, K. Strunz, A review of modeling, management, and applications of grid connected Li ion battery storage systems, IEEE Trans. Smart Grid 13 (6) (2022) 4505–4524, https://doi.org/10.1109/TSG.2022.3188598.
[3] X. Zhang, Y. Yang, Z. Zhou, Towards practical lithium-metal anodes, Chem. Soc. Rev. 49 (2020) 3040–3071.
[4] M. Zhao, B.-Q. Li, X.-Q. Zhang, J.-Q. Huang, Q. Zhang, A perspective toward practical lithium–sulfur batteries, ACS Cent. Sci. 6 (2020) 1095–1104.
[5] W.-J. Kwak, D. Sharon Rosy, C. Xia, H. Kim, L.R. Johnson, P.G. Bruce, L.F. Nazar, Y.-K. Sun, A.A. Frimer, Lithium–oxygen batteries and related systems: potential, status, and future, Chem. Rev. 120 (2020) 6626–6683.
[6] S. Huang, Z. Wang, Y. Von Lim, Y. Wang, Y. Li, D. Zhang, H.Y. Yang, Recent advances in heterostructure engineering for lithium–sulfur batteries, Adv. Energy Mater. 11 (2021) 2003689.
[7] C. Xia, C.Y. Kwok, L.F. Nazar, A high-energy-density lithium-oxygen battery based on a reversible four-electron conversion to lithium oxide, Science 361 (2018) (1979) 777–781.
[8] J. He, A. Manthiram, A review on the status and challenges of electrocatalysts in lithium-sulfur batteries, Energy Storage Mater. 20 (2019) 55–70.
[9] D. Su, D. Zhou, C. Wang, G. Wang, Toward high performance lithium–sulfur batteries based on Li_2S cathodes and beyond: status, challenges, and perspectives, Adv. Funct. Mater. 28 (2018) 1800154.
[10] X. Huang, Z. Wang, R. Knibbe, B. Luo, S.A. Ahad, D. Sun, L. Wang, Cyclic voltammetry in lithium–sulfur batteries—challenges and opportunities, Energ. Technol. 7 (2019) 1801001.
[11] Y. Huang, L. Lin, C. Zhang, L. Liu, Y. Li, Z. Qiao, J. Lin, Q. Wei, L. Wang, Q. Xie, Recent advances and strategies toward polysulfides shuttle inhibition for high-performance Li–S batteries, Adv. Sci. 9 (2022) 2106004.
[12] A.N. Mistry, P.P. Mukherjee, "Shuttle" in polysulfide shuttle: friend or foe? J. Phys. Chem. C 122 (2018) 23845–23851.

[13] W. Tian, H. Zhang, X. Duan, H. Sun, G. Shao, S. Wang, Porous carbons: structure-oriented design and versatile applications, Adv. Funct. Mater. 30 (2020) 1909265.
[14] J. Cheng, Y. Liu, X. Zhang, X. Miao, Y. Chen, S. Chen, J. Lin, Y. Zhang, Structure engineering in interconnected porous hollow carbon spheres with superior rate capability for supercapacitors and lithium-sulfur batteries, Chem. Eng. J. 419 (2021), 129649.
[15] J. Kang, X. Tian, C. Yan, L. Wei, L. Gao, J. Ju, Y. Zhao, N. Deng, B. Cheng, W. Kang, Customized structure design and functional mechanism analysis of carbon spheres for advanced lithium–sulfur batteries, Small 18 (2022) 2104469.
[16] A.A. Razzaq, Y. Yao, R. Shah, P. Qi, L. Miao, M. Chen, X. Zhao, Y. Peng, Z. Deng, High-performance lithium sulfur batteries enabled by a synergy between sulfur and carbon nanotubes, Energy Storage Mater. 16 (2019) 194–202.
[17] M. Zheng, Y. Chi, Q. Hu, H. Tang, X. Jiang, L. Zhang, S. Zhang, H. Pang, Q. Xu, Carbon nanotube-based materials for lithium–sulfur batteries, J. Mater. Chem. A Mater. 7 (2019) 17204–17241.
[18] Q. Li, Y. Liu, L. Yang, Y. Wang, Y. Liu, Y. Chen, X. Guo, Z. Wu, B. Zhong, N, O co-doped chlorella-based biomass carbon modified separator for lithium-sulfur battery with high capacity and long cycle performance, J. Colloid Interface Sci. 585 (2021) 43–50.
[19] Q. Xiao, G. Li, M. Li, R. Liu, H. Li, P. Ren, Y. Dong, M. Feng, Z. Chen, Biomass-derived nitrogen-doped hierarchical porous carbon as efficient sulfur host for lithium–sulfur batteries, J. Energy Chem. 44 (2020) 61–67.
[20] Z. Gu, C. Cheng, T. Yan, G. Liu, J. Jiang, J. Mao, K. Dai, J. Li, J. Wu, L. Zhang, Synergistic effect of Co_3Fe_7 alloy and N-doped hollow carbon spheres with high activity and stability for high-performance lithium-sulfur batteries, Nano Energy 86 (2021), 106111.
[21] Z. Xiao, Z. Yang, Z. Li, P. Li, R. Wang, Synchronous gains of areal and volumetric capacities in lithium–sulfur batteries promised by flower-like porous $Ti_3C_2T_x$ matrix, ACS Nano 13 (2019) 3404–3412.
[22] G. Xia, J. Ye, Z. Zheng, X. Li, C. Chen, C. Hu, Catalytic FeP decorated carbon black as a multifunctional conducting additive for high-performance lithium-sulfur batteries, Carbon N. Y. 172 (2021) 96–105.
[23] H. Pan, K.S. Han, M.H. Engelhard, R. Cao, J. Chen, J. Zhang, K.T. Mueller, Y. Shao, J. Liu, Addressing passivation in lithium–sulfur battery under lean electrolyte condition, Adv. Funct. Mater. 28 (2018) 1707234.
[24] B. Ma, Y. Gao, M. Niu, M. Luo, H. Li, Y. Bai, K. Sun, ZIF-67/Super P modified separator as an efficient polysulfide barrier for high-performance lithium-sulfur batteries, Solid State Ion. 371 (2021), 115750.
[25] S. Li, W. Zhang, J. Zheng, M. Lv, H. Song, L. Du, Inhibition of polysulfide shuttles in Li–S batteries: modified separators and solid-state electrolytes, Adv. Energy Mater. 11 (2021) 2000779.
[26] L. Jin, B. Huang, X. Qian, J. Chen, J. Cheng, Q. Hao, K. Zhang, Hollow bimetallic sulfide composite coated separator for hindering the shuttle of polysulfides in Li-S batteries, J. Alloys Compd. 926 (2022), 166515.
[27] X. Wang, Y. Wang, F. Wu, G. Jin, J. Li, Z. Zhang, Continuous zirconium-based MOF-808 membranes for polysulfide shuttle suppression in lithium-sulfur batteries, Appl. Surf. Sci. 153628 (2022).
[28] C.-J. Huang, J.-H. Cheng, W.-N. Su, P. Partovi-Azar, L.-Y. Kuo, M.-C. Tsai, M.-H. Lin, S.P. Jand, T.-S. Chan, N.-L. Wu, Origin of shuttle-free sulfurized polyacrylonitrile in lithium-sulfur batteries, J. Power Sources 492 (2021), 229508.
[29] X. Chen, L. Peng, L. Wang, J. Yang, Z. Hao, J. Xiang, K. Yuan, Y. Huang, B. Shan, L. Yuan, Ether-compatible sulfurized polyacrylonitrile cathode with excellent performance enabled by fast kinetics via selenium doping, Nat. Commun. 10 (2019) 1–9.
[30] W. Wang, Z. Cao, G.A. Elia, Y. Wu, W. Wahyudi, E. Abou-Hamad, A.-H. Emwas, L. Cavallo, L.-J. Li, J. Ming, Recognizing the mechanism of sulfurized polyacrylonitrile cathode materials for Li–S batteries and beyond in Al–S batteries, ACS Energy Lett. 3 (2018) 2899–2907.
[31] X. Wang, Y. Qian, L. Wang, H. Yang, H. Li, Y. Zhao, T. Liu, Sulfurized polyacrylonitrile cathodes with high compatibility in both ether and carbonate electrolytes for ultrastable lithium–sulfur batteries, Adv. Funct. Mater. 29 (2019) 1902929.
[32] W. Chen, B. Li, C. Zhao, M. Zhao, T. Yuan, R. Sun, J. Huang, Q. Zhang, Electrolyte regulation towards stable lithium-metal anodes in lithium–sulfur batteries with sulfurized polyacrylonitrile cathodes, Angew. Chem. Int. Ed. 59 (2020) 10732–10745.
[33] X. Zhao, C. Wang, Z. Li, X. Hu, A.A. Razzaq, Z. Deng, Sulfurized polyacrylonitrile for high-performance lithium sulfur batteries: advances and prospects, J. Mater. Chem. A Mater. 9 (2021) 19282–19297.
[34] H. Li, W. Xue, W. Xu, L. Wang, T. Liu, Controllable synthesis of sulfurized polyacrylonitrile nanofibers for high performance lithium–sulfur batteries, Compos. Commun. 24 (2021), 100675.
[35] J. Xiang, Z. Guo, Z. Yi, Y. Zhang, L. Yuan, Z. Cheng, Y. Shen, Y. Huang, Facile synthesis of sulfurized polyacrylonitrile composite as cathode for high-rate lithium-sulfur batteries, J. Energy Chem. 49 (2020) 161–165.
[36] S. Dalton, F. Heatley, P.M. Budd, Thermal stabilization of polyacrylonitrile fibres, Polymer (Guildf). 40 (1999) 5531–5543.
[37] Y. Wang, L. Xu, M. Wang, W. Pang, X. Ge, Structural identification of polyacrylonitrile during thermal treatment by selective ^{13}C labeling and solid-state ^{13}C NMR spectroscopy, Macromolecules 47 (2014) 3901–3908.
[38] X. Liu, Y. Makita, Y. Hong, Y. Nishiyama, T. Miyoshi, Chemical reactions and their kinetics of atactic-polyacrylonitrile as revealed by solid-state ^{13}C NMR, Macromolecules 50 (2017) 244–253.
[39] M.S.A. Rahaman, A.F. Ismail, A. Mustafa, A review of heat treatment on polyacrylonitrile fiber, Polym. Degrad. Stab. 92 (2007) 1421–1432, https://doi.org/10.1016/j.polymdegradstab. 2007.03.023.
[40] J. Fanous, M. Wegner, J. Grimminger, A. Andresen, M.R. Buchmeiser, Structure-related electrochemistry of sulfur-poly (acrylonitrile) composite cathode materials for rechargeable lithium batteries, Chem. Mater. 23 (2011) 5024–5028.
[41] M. Frey, R.K. Zenn, S. Warneke, K. Müller, A. Hintennach, R.E. Dinnebier, M. R. Buchmeiser, Easily accessible, textile fiber-based sulfurized poly (acrylonitrile) as Li/S cathode material: correlating electrochemical performance with morphology and structure, ACS Energy Lett. 2 (2017) 595–604.
[42] X. Zhao, C. Wang, Z. Li, X. Hu, A.A. Razzaq, Z. Deng, Sulfurized polyacrylonitrile for high-performance lithium sulfur batteries: advances and prospects, J. Mater. Chem. A Mater. 9 (2021) 19282–19297.
[43] J. Lei, J. Chen, H. Zhang, A. Naveed, J. Yang, Y. Nuli, J. Wang, High molecular weight polyacrylonitrile precursor for S@ pPAN composite cathode materials with high specific capacity for rechargeable lithium batteries, ACS Appl. Mater. Interfaces 12 (2020) 33702–33709.
[44] X. Han, X. Wang, M. Han, J. Sun, A full battery system of pre-lithiated phosphorus/sulfurized pyrolyzed poly (acrylonitrile) with an effective electrolyte and improved safety, Green Chem. 22 (2020) 4252–4258.
[45] X. Chen, L. Peng, L. Wang, J. Yang, Z. Hao, J. Xiang, K. Yuan, Y. Huang, B. Shan, L. Yuan, Ether-compatible sulfurized polyacrylonitrile cathode with excellent performance enabled by fast kinetics via selenium doping, Nat. Commun. 10 (2019) 1–9.
[46] Z. Shen, W. Zhang, S. Mao, S. Li, X. Wang, Y. Lu, Tailored electrolytes enabling practical lithium–sulfur full batteries via interfacial protection, ACS Energy Lett. 6 (2021) 2673–2681.
[47] S. Li, Z. Han, W. Hu, L. Peng, J. Yang, L. Wang, Y. Zhang, B. Shan, J. Xie, Manipulating kinetics of sulfurized polyacrylonitrile with tellurium as eutectic accelerator to prevent polysulfide dissolution in lithium-sulfur battery under dissolution-deposition mechanism, Nano Energy 60 (2019) 153–161.
[48] S. Wei, L. Ma, K.E. Hendrickson, Z. Tu, L.A. Archer, Metal–sulfur battery cathodes based on PAN–sulfur composites, J. Am. Chem. Soc. 137 (2015) 12143–12152.
[49] Y. Zhang, Y. Sun, L. Peng, J. Yang, H. Jia, Z. Zhang, B. Shan, J. Xie, Se as eutectic accelerator in sulfurized polyacrylonitrile for high performance all-solid-state lithium-sulfur battery, Energy Storage Mater. 21 (2019) 287–296.
[50] S. Ma, Z. Zhang, Y. Wang, Z. Yu, C. Cui, M. He, H. Huo, G. Yin, P. Zuo, Iodine-doped sulfurized polyacrylonitrile with enhanced electrochemical performance for lithium sulfur batteries in carbonate electrolyte, Chem. Eng. J. 418 (2021), 129410.
[51] A.A. Razzaq, X. Yuan, Y. Chen, J. Hu, Q. Mu, Y. Ma, X. Zhao, L. Miao, J.-H. Ahn, Y. Peng, Anchoring MOF-derived CoS_2 on sulfurized polyacrylonitrile nanofibers for high areal capacity lithium–sulfur batteries, J. Mater. Chem. A Mater. 8 (2020) 1298–1306.
[52] X. Li, Y. Liu, C. Lin, Y. Wang, Z. Lei, P. Xiong, Y. Luo, Q. Chen, L. Zeng, M. Wei, Structure engineering of BiSbSx nanocrystals embedded within sulfurized polyacrylonitrile fibers for high performance of potassium-ion batteries, Chem. Eur. J. 28 (2022), e202200028.
[53] T.N.L. Doan, M. Ghaznavi, Y. Zhao, Y. Zhang, A. Konarov, M. Sadhu, R. Tangirala, P. Chen, Binding mechanism of sulfur and dehydrogenated polyacrylonitrile in sulfur/polymer composite cathode, J. Power Sources 241 (2013) 61–69.
[54] S. Wei, L. Ma, K.E. Hendrickson, Z. Tu, L.A. Archer, Metal–sulfur battery cathodes based on PAN–sulfur composites, J. Am. Chem. Soc. 137 (2015) 12143–12152.
[55] N. Sapkota, S. Chiluwal, P. Parajuli, A. Rowland, R. Podila, Insights into the pseudocapacitive behavior of sulfurized polymer electrodes for Li–S batteries, Adv. Sci. 10 (2023) 2206901, https://doi.org/10.1002/advs.202206901.
[56] C.-J. Huang, K.-Y. Lin, Y.-C. Hsieh, W.-N. Su, C.-H. Wang, G. Brunklaus, M. Winter, J.-C. Jiang, B.J. Hwang, New insights into the N–S bond formation of a sulfurized-polyacrylonitrile cathode material for lithium–sulfur batteries, ACS Appl. Mater. Interfaces 13 (2021) 14230–14238.
[57] S. Bertolini, T. Jacob, Sulfurized-polyacrylonitrile in lithium-sulfur batteries: interactions between undercoordinated carbons and polymer structure under low lithiation, J. Energy Chem. 66 (2022) 587–596, https://doi.org/10.1016/j.jechem.2021.08.070.
[58] S. Perez Beltran, P.B. Balbuena, Sulfurized polyacrylonitrile for high-performance lithium–sulfur batteries: in-depth computational approach revealing multiple sulfur's reduction pathways and hidden Li^+ storage mechanisms for extra discharge capacity, ACS Appl. Mater. Interfaces 13 (2021) 491–502. doi:https://doi.org/10.1021/acsami.0c17537.
[59] J. Guo, Z. Yang, Y. Yu, H.D. Abruña, L.A. Archer, Lithium–sulfur battery cathode enabled by lithium–nitrile interaction, J. Am. Chem. Soc. 135 (2013) 763–767.
[60] S. Bertolini, T. Jacob, Density functional theory studies on sulfur–polyacrylonitrile as a cathode host material for lithium–sulfur batteries, ACS Omega 6 (2021) 9700–9708, https://doi.org/10.1021/acsomega.0c06240.
[61] S. Bertolini, T. Jacob, Capturing polysulfides by sulfurized-polyacrylonitrile in lithium-sulfur batteries and the sulfur-chain effects through Density Functional Theory, Electrochem. Sci. Adv. 2 (2022), e2100129, https://doi.org/10.1002/elsa.202100129.
[62] S. Bertolini, T. Jacob, Atomistic discharge studies of sulfurized-polyacrylonitrile through ab initio molecular dynamics, Electrochim. Acta 403 (2022), 139538, https://doi.org/10.1016/j.electacta.2021.139538.
[63] S. Grimme, S. Ehrlich, L. Goerigk, Effect of the damping function in dispersion corrected density functional theory, J. Comput. Chem. 32 (2011) 1456–1465.
[64] D.M. Bylander, L. Kleinman, Energy fluctuations induced by the Nosé thermostat, Phys. Rev. B 46 (1992) 13756.
[65] N. Shuichi, Constant temperature molecular dynamics methods, Prog. Theor. Phys. Suppl. 103 (1991) 1–46.
[66] S. Nosé, A unified formulation of the constant temperature molecular dynamics methods, J. Chem. Phys. 81 (1984) 511–519.

[67] H.J. Monkhorst, J.D. Pack, Special points for Brillouin-zone integrations, Phys. Rev. B 13 (1976) 5188.
[68] G. Kresse, D. Joubert, From ultrasoft pseudopotentials to the projector augmented-wave method, Phys. Rev. B. 59 (1999) 1758.
[69] P.E. Blöchl, Projector augmented-wave method, Phys. Rev. B. 50 (1994) 17953.
[70] R. Car, M. Parrinello, Unified approach for molecular dynamics and density-functional theory, Phys. Rev. Lett. 55 (1985) 2471.
[71] M.C. Payne, M.P. Teter, D.C. Allan, T.A. Arias, J.D. Joannopoulos, Iterative minimization techniques for ab initio total-energy calculations: molecular dynamics and conjugate gradients, Rev. Mod. Phys. 64 (1992) 1045.
[72] G. Kresse, J. Hafner, Ab initio molecular dynamics for open-shell transition metals, Phys. Rev. B 48 (1993) 13115.
[73] G. Kresse, J. Furthmüller, Efficient iterative schemes for ab initio total-energy calculations using a plane-wave basis set, Phys. Rev. B. 54 (1996) 11169.
[74] F. Wu, S. Thieme, A. Ramanujapuram, E. Zhao, C. Weller, H. Althues, S. Kaskel, O. Borodin, G. Yushin, Toward in-situ protected sulfur cathodes by using lithium bromide and pre-charge, Nano Energy 40 (2017) 170–179, https://doi.org/10.1016/j.nanoen.2017.08.012.
[75] F. Neese, The ORCA program system, Wiley Interdiscip. Rev. Comput. Mol. Sci. 2 (2012) 73–78.
[76] F. Neese, Software update: the ORCA program system—version 5.0, Wiley Interdiscip. Rev. Comput. Mol. Sci. 12 (2022), e1606.
[77] O. Borodin, W. Behl, T.R. Jow, Oxidative stability and initial decomposition reactions of carbonate, sulfone, and alkyl phosphate-based electrolytes, J. Phys. Chem. C 117 (2013) 8661–8682.
[78] L.E. Camacho-Forero, P.B. Balbuena, Elucidating electrolyte decomposition under electron-rich environments at the lithium-metal anode, Phys. Chem. Chem. Phys. 19 (2017) 30861–30873.
[79] F. Wu, J.T. Lee, N. Nitta, H. Kim, O. Borodin, G. Yushin, Lithium iodide as a promising electrolyte additive for lithium–sulfur batteries: mechanisms of performance enhancement, Adv. Mater. 27 (2015) 101–108.
[80] O. Borodin, M. Olguin, C.E. Spear, K.W. Leiter, J. Knap, Towards high throughput screening of electrochemical stability of battery electrolytes, Nanotechnology 26 (2015), 354003.
[81] L. Xing, O. Borodin, G.D. Smith, W. Li, Density functional theory study of the role of anions on the oxidative decomposition reaction of propylene carbonate, J. Phys. Chem. A 115 (2011) 13896–13905, https://doi.org/10.1021/jp206153n.
[82] L. Xing, O. Borodin, Oxidation induced decomposition of ethylene carbonate from DFT calculations — importance of explicitly treating surrounding solvent, Phys. Chem. Chem. Phys. 14 (2012) 12838–12843, https://doi.org/10.1039/C2CP41103B.
[83] O. Borodin, Challenges with prediction of battery electrolyte electrochemical stability window and guiding the electrode–electrolyte stabilization, Curr. Opin. Electrochem. 13 (2019) 86–93, https://doi.org/10.1016/j.coelec.2018.10.015.
[84] C.-J. Huang, J.-H. Cheng, W.-N. Su, P. Partovi-Azar, L.-Y. Kuo, M.-C. Tsai, M.-H. Lin, S.P. Jand, T.-S. Chan, N.-L. Wu, Origin of shuttle-free sulfurized polyacrylonitrile in lithium-sulfur batteries, J. Power Sources 492 (2021), 229508.
[85] M.A. Weret, C.-F.J. Kuo, T.S. Zeleke, T.T. Beyene, M.-C. Tsai, C.-J. Huang, G. B. Berhe, W.-N. Su, B.-J. Hwang, Mechanistic understanding of the sulfurized-poly (acrylonitrile) cathode for lithium-sulfur batteries, Energy Storage Mater. 26 (2020) 483–493.